Eur. Phys. J. C 49, 261–267 (2007)
DOI 10.1140/epjc/s10052-006-0097-2

THE EUROPEAN PHYSICAL JOURNAL C

Regular Article – Experimental Physics

Di-electron production in C+C and p+p collisions with HADES

T. Eberl[a] for the HADES Collaboration

Physik Department E12, Technische Universität München, James-Franck-Str. 1, 85748 Garching, Germany

Received: 29 July 2006 /
Published online: 27 October 2006 – © Springer-Verlag / Società Italiana di Fisica 2006

Abstract. The High Acceptance Di-Electron Spectrometer HADES at GSI, Darmstadt, has been designed for systematic studies of hadron properties inside nuclear matter. First measured mass and momentum distributions of e^+e^- pairs produced in ^{12}C+^{12}C collisions at 1 and 2 AGeV are presented and compared with p+p collisions at 2.2 GeV incident energy. The spectrometer set-up and the analysis methods are briefly outlined and a comparison of the data with Monte-Carlo events from a generator based on known production cross-sections and branching ratios is shown and discussed.

1 Introduction

Di-electrons represent a unique and ideally suited probe to study the properties of hadrons inside nuclear matter and of nuclear matter itself, as they do not undergo strong distorting final state interactions. Relativistic nuclear collisions are used to create a hadronic medium at elevated temperatures and densities, whereas beams of pions and protons impinging on cold nuclei are suited to investigate hadrons at normal nuclear matter density. Several theoretical models predict a significant change of the masses and widths of light vector mesons ρ/ω in high density and high temperature nuclear matter. As an example, Brown–Rho [1, 2] scaling predicts a decrease of the vector meson pole masses proportional to the density of the medium. Models based on QCD sum rules [3] and effective hadronic models [4] reach similar conclusions, but rather stress the broadening of the meson spectral functions. Hence, experimental studies of possible modifications of meson properties inside the nuclear medium have been a hot topic in nuclear physics over the past decade and before. While the dilepton spectra in ultrarelativistic heavy-ion collisions can be reasonably well described by the most recent theoretical models, significant discrepancies between theory and experiment still persist for the energy regime of a few GeV per nucleon kinetic beam energy.

Di-electron and di-muon spectra have been measured at the CERN SPS by the CERES [5], HELIOS [6] and NA60 [7] collaborations at various energies up to 158 AGeV. The recent NA60 high-resolution di-muon spectra seem to rule out a mere dropping mass scenario as an explanation for the earlier observed significant enhancement of dilepton yield below the $\rho-\omega$ region.The data rather support the picture of a broadened $\rho-\omega$ in-medium spectral function. The enhanced strength below the ω-peak observed in γ-nucleus [8] and proton–nucleus [9] reactions has also been interpreted as a possible in-medium effect. In the lower BEVALAC energy regime di-electron invariant-mass distributions have been measured in proton–proton, light and heavy ion reactions by the DLS collaboration [10, 11]. Within the experimental error bars the extracted e^+e^- production rates in proton-proton reactions could be reasonably well reproduced by calculations assuming free di-electron decays of various hadronic sources [12–14]. For the nuclear collision systems Ca+Ca and C+C, however, a remarkable excess of the di-electron yield was found in the low mass range $200\,\mathrm{MeV/c^2} < M < 600\,\mathrm{MeV/c^2}$ as compared to the theoretical calculations. So far, this di-electron excess could not be described satisfactorily by any of the models. Although a recent attempt utilizing the excitation of nucleon resonances within the framework of an extended Vector Meson Dominance model (eVMD) [15, 16] improves the description of the available data set considerably, the so-called DLS puzzle persists.

The HADES collaboration has therefore started its physics program by revisiting both, the p+p and the nuclear collision systems C+C and Ca+Ca at beam energies up to 2 AGeV, with the aim to enlarge and broaden the experimental data sample by high resolution data with significantly improved signal to background ratio.

2 Experimental set-up and e^+e^--signal reconstruction

In the design of the HADES spectrometer, which is described in detail elsewhere [17, 18], particular emphasis was put to a mass resolution of $\Delta M_{\mathrm{inv}}/M_{\mathrm{inv}} \simeq 1\%(\sigma)$ and a good signal-to-background ratio. Besides this, the capability to accept high data rates to cope with the low production cross sections and the small electromagnetic

[a] email: Thomas.Eberl@ph.tum.de

decay branching ratios is indispensable. It consists therefore of a 6-coil toroidal magnet centered on the beam axis and six identical detection sections mounted between the coils which cover polar angles between 18° and 85°. A segmented time of flight wall (TOF+TOFino) [22] is used to generate a fast collision trigger signal (LVL1) based on the registered charged particle multiplicity. In addition it discriminates hadrons from electrons, supported by a PreSHOWER detector [23] at forward polar angles for high momentum $e^{\pm}$ with $p > 0.5\,\mathrm{GeV/c}$. Four planes of multi-wire drift chambers (MDCs) [21] together with the superconducting magnet serve as a high resolution tracking system for the momentum measurement. A fast and hadron blind ring imaging Cherenkov detector (RICH) [19, 20] in the field free region around the target is the central identification device for e^+e^--pairs. It is equipped with a C_4F_{10} gas radiator with a Cherenkov threshold of $\gamma_{\mathrm{thresh}} = 18.3$, which ensures electron detection for momenta $p > 0.05\,\mathrm{GeV/c}$ and excludes radiation from hadrons at SIS beam energies. The Cherenkov photons are focused by a spherical mirror onto a position-sensitive photon detector to ring images of constant radius. From the reconstructed ring centers, the polar (θ) and azimuthal (ϕ) coordinates of the electron trajectory with respect to the collision vertex are calculated and then correlated with particle trajectories measured by the tracking system and the hit coordinates in the TOF and PreSHOWER detectors. With an additional threshold on the particle time of flight a second trigger (LVL2) decision [24, 25] is generated online, in order to identify events with at least one e^+ or e^-. It was shown by Monte-Carlo simulations that this spectrometer geometry results in a nearly flat di-electron acceptance of $A_{e^+e^-} \simeq 30\%$ for pairs with invariant masses $M < 1.5\,\mathrm{GeV/c^2}$ and transverse momenta $P_\perp < 1.5\,\mathrm{GeV/c}$ [17].

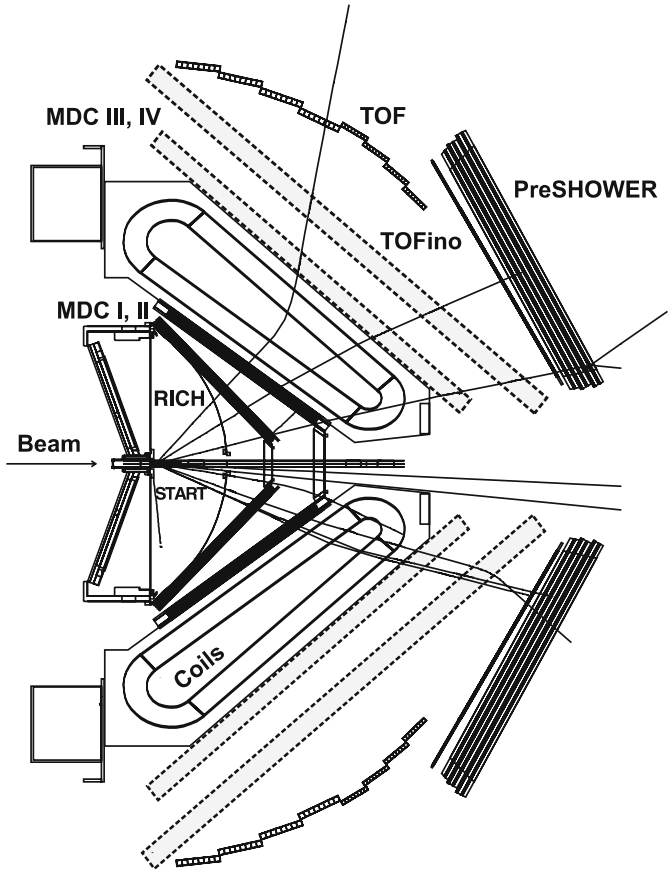

Fig. 1. Side view of the HADES set-up. The upper- and lowermost of the altogether 6 sectors are depicted, with individual detectors and magnet coils included schematically. The tracks resemble a simulated C+C event. High resolution tracking requires the MDC planes III and IV which were not available for the C+C at $E = 2$ AGeV experiment

The e^+e^--signal reconstruction starts with the track reconstruction and identification of single $e^{\pm}$ and proceeds in four main steps. First $e^{\pm}$ are identified on the basis of their ring signatures in the RICH. Moreover, the emission angle of the electron trajectory inside the RICH is determined. Second, track segments are reconstructed in the different chambers of the MDC. Then the TOF and PreSHOWER detector hits are reconstructed and evaluated to discriminate electrons and hadrons behind the magnetic field. In the last step the found detector hits are matched in coordinate space and an appropriate track model is fitted to the matched MDC track segments, in order to determine the particle momentum. For the assignment of a particular particle type to a fitted track 2 different approaches have been evaluated and both are used successfully. The first method cuts on detector signals and single particle quantities with adaptive window sizes in 1- and 2-dimensional distributions. The second implements a more sophisticated algorithm based on a probabilistic approach following Bayes' theorem. Detector signals and single track properties such as the time-of-flight or the energy loss in a detector material are used to determine the relative probabilities of a track to be a $e^{\pm}$, $\pi^{\pm}$, p or d. Both methods were found to provide roughly the same high single particle purities, while the efficiency to find a given $e^{\pm}$ in the simulation was found to be higher for the method based on Bayes' theorem.

The e^+e^--pair reconstruction is then achieved by the combination of fitted and identified single $e^{\pm}$ candidate tracks. In a first step, all tracks are removed from the event which do not contain a unique set of detector hits, i.e. tracks with detector hits that were used more than once in the reconstruction of a particle track. Next, all lepton tracks are discarded from the event which are closer than 9° to another particle candidate (hadron or lepton) or a track segment that could not be fitted successfully. Finally, like-sign (e^+e^+ and e^-e^-) and opposite-sign (e^+e^-) pairs are constructed systematically from all remaining tracks of the event.

3 Di-electron production in C+C collisions

3.1 C+C at $E = 2$ AGeV

In the first production run of HADES a carbon beam of 10^6 particles/s was directed to a segmented carbon

target of $2 \times 2.5\%$ interaction length. Since the experiment was performed before completion of the construction phase, the MDC planes III and IV behind the magnetic field were not yet available. The data readout was started by the LVL1 trigger decision requiring a charged-particle multiplicity of MUL ≥ 4 in the TOF/TOFino detectors coincident to a fast timing signal from a diamond beam detector located upstream of the target. A second-level trigger based on online pattern recognition in the RICH was used to enhance the di-electron event statistics. The attained enhancement in $e^{\pm}$ content per event was about one order of magnitude as compared to a LVL1 event [24, 25]. The achieved momentum resolution of $\sigma_{\rm p}/p = 0.02 + 0.13p\,[{\rm GeV/c}]$ was dominated by the granularity of the TOF and PreSHOWER detectors, which were used for particle trajectory determination behind the magnetic field. The momentum resolution translates into an invariant-mass resolution of $\sigma_{\rm M}/M = 9\%$ at $M = 0.8\,{\rm GeV/c^2}$. The results presented below were obtained from a total statistics of 6.5×10^8 LVL1 events.

The lepton track reconstruction proceeded as described above. For the particle identification straight forward cuts on detector observables were used. The coordinates of ring centers in the RICH were correlated with corresponding angles of track segments reconstructed in the inner MDC detectors. The correlation windows are determined by the RICH position resolution of 3 mm. The $e^{\pm}$ track candidates were matched with those hits in the TOF or TOFino/PreSHOWER detectors which fulfilled electron conditions, i.e. (a) a particle velocity of $\beta = 1 \pm 3\sigma_{\beta}$, where σ_{β} is given by the time-of-flight resolution [22], and (b) an electromagnetic shower signature in the PreSHOWER [23]. Finally, the particle momentum was determined from the deflection in the known magnetic field by a fit of all track coordinates.

From the sample of single $e^{\pm}$ track candidates opposite-sign (e^+e^-) pairs were formed to extract opening angle and invariant-mass distributions. A considerable fraction of these pairs, however, emerges as combinatorial background (CB). The CB is mostly due to uncorrelated electrons produced by external pair conversion of photons from $\pi^0 \to \gamma\gamma$ and/or $\pi^0 \to e^+e^-\gamma$ Dalitz decays. The conversion pairs are produced either in the target or in the RICH radiator and have small opening angles ($\theta^{\rm conv}_{e+e-} < 9^{\circ}$) which often lead to partially overlapping tracks in the inner tracking system. Hence, a large fraction of these pairs could be rejected efficiently by applying conditions on the opening angle and on the fit quality (χ^2) of the reconstructed track segments. It was shown by simulation that this procedure already removes 95% of the conversion pairs while reducing the interesting di-electron signal with $M > 0.15\,{\rm GeV/c^2}$ by less than 10%.

Figure 2 shows the resulting invariant-mass distribution of the e^+e^- pairs, decomposed into its physics signal part and a still remaining combinatorial background contribution. The remaining background was obtained from like-sign pairs detected in the same event and calculated by the geometric mean $N_{\rm CB} = 2\sqrt{N_{e^+e^+}N_{e^-e^-}}$ of the reconstructed invariant-mass distributions ${\rm d}N_{e^+e^+}/{\rm d}M$ and

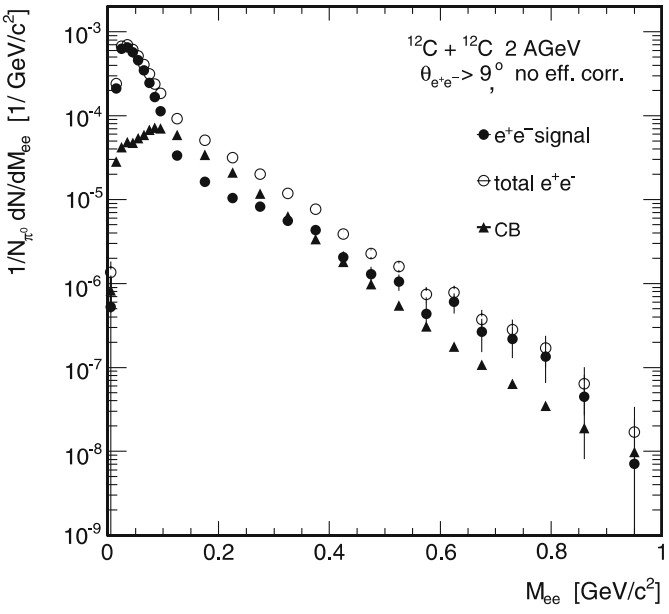

Fig. 2. Reconstructed e^+e^- invariant-mass distributions (*open circles*) for pairs with opening angles $\theta_{e+e-} > 9^{\circ}$. The signal distribution (*full circles*) was obtained by subtracting the combinatorial background (*triangles*). Note that the spectrum is neither corrected for acceptance nor for efficiency. The displayed error bars are statistical only

${\rm d}N_{e^-e^-}/{\rm d}M$. However, in the high mass region ($M > 0.5\,{\rm GeV/c^2}$) the number of like sign pairs was too small to obtain a reliable background signal. Therefore, we used for this part the event mixing procedure for background reconstruction. Uncorrelated opposite-sign e^+e^- pairs were built with tracks from different events but originating from reaction vertices in the same target segment. It was verified that in the mass region $0.15 < M < 0.5\,{\rm GeV/c^2}$ the CB distributions obtained from event mixing and the same-event like-sign pairs agree within 10% when normalized to the same yield.

After CB subtraction, a total of ~ 23000 signal pairs (~ 2000 with $M_{e+e-} > 0.15\,{\rm GeV/c^2}$) were reconstructed. The signal-to-background ratio (S/B) was found to be roughly 10 for the π^0 mass range, 1 for the intermediate mass range up to $0.5\,{\rm GeV/c^2}$ and 2–3 for the higher masses. These values are significantly better than in any previous di-electron measurement. The distributions in Fig. 2 were normalized to the average number of neutral pions N_{π^0} per collision. Its value was extracted independently from the number of charged pions $N_{\pi} = \frac{1}{2}(N_{\pi^+} + N_{\pi^-})$ measured simultaneously in the HADES acceptance. For the normalisation we assume that N_{π} can be regarded as a measure of the π^0 multiplicity N_{π^0}, since the collision system ^{12}C+^{12}C is isospin-symmetric. The necessary extrapolation to the full solid angle was based on the results of transport calculations [26], which reproduce the measured angular distributions correctly. In addition, the extrapolated charged-pion yields $N_{\pi}^{4\pi}$ (with $N_{\pi}^{4\pi}/A_{\rm part} = 0.137 \pm 0.015$) obtained in our experiment agree with previous measurements [27, 28] within the quoted error of 11%.

The correction factors for detector and reconstruction inefficiencies were determined by Monte-Carlo simulations. Single electron tracks with uniform and isotropic distributions in momentum and emission angle were embedded in simulated events of the UrQMD transport model [26]. Realistic detector responses were generated by means of a detailed GEANT simulation. Finally, the digitized events were processed through the same analysis chain as the experimental data and the probability to correctly reconstruct an embedded single $e^{\pm}$ track was determined. The pair efficiency E_{+-} was calculated as the product of the single-electron efficiencies, i.e. $E_{+-} = \epsilon_{+}\epsilon_{-}$ for given electron momenta and emission angles. It was verified that within an uncertainty of 20% the single track efficiencies are independent for pairs with opening angles larger than 9°. The experimental data were then corrected on a pair-by-pair basis with the weighting factor $1/E_{+-}$. The CB distributions were treated in the same way and then subtracted from the total pair signal, as described above. The geometrical pair acceptance of the HADES detector was obtained in analogy to the pair efficiency as product of the single-electron acceptances $A_{\pm}(p, \theta, \phi)$. No attempt, however, was made so far to extrapolate the measured electron yields to the full solid angle.

Figure 3 (circles) shows the efficiency corrected $e^{+}e^{-}$ invariant-mass distribution as the net signal after background subtraction. The displayed error bars represent the statistical errors only. Remaining uncertainties in the efficiency corrections and the CB determination lead to an additional systematic error of roughly 30% . Corresponding transverse momentum and rapidity distributions are depicted in Figs. 4 and 5, respectively. The distributions are plotted for all signal pairs and for those with masses $M > 0.15\,\mathrm{GeV/c^2}$. In both cases a clear change in the shape of the distributions is visible, when the π^0 mesons are excluded. The smaller slope parameter in the $P_{\perp}$ distribution and the more pronounced symmetry around mid rapidity indicate that the $e^{+}e^{-}$-sources contributing to the high mass sample may experience a different thermalisation scenario as do the neutral pions.

To get first insights and before performing transport model calculations we compare the experimental data to a simulation based on an incoherent sum (cocktail) of simulated di-electron sources created with the event generator PLUTO [29]. The first cocktail was composed of free π^0 and η (solid lines), only. The π^0 and η meson production in ^{12}C+^{12}C collisions is known from systematic measurements of their 2-photon decay branches [27]. In PLUTO, the meson production was parametrised by assuming the anisotropic emission from a thermal source with a temperature $T = 80\,\mathrm{MeV}$, but no radial expansion velocity. The generated pairs were filtered through the HADES geometrical acceptance and normalized to the simulated π^0 multiplicity. The simulated distribution is in fair agreement in the π^0 mass region, but undershoots the data above $M > 0.15\,\mathrm{GeV/c^2}$ significantly. This indicates that additional sources have to be taken into account, such as short-lived baryon resonances (mainly $\Delta(1232)$) and/or vector mesons. These contributions are of particular interest since – at these beam energies – they may represent

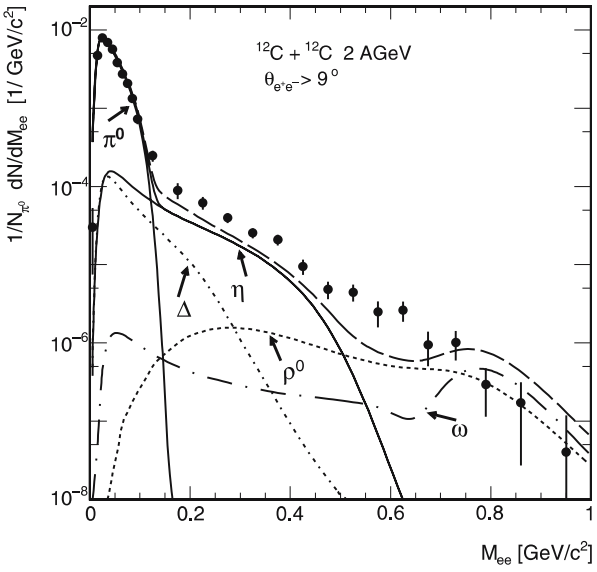

Fig. 3. Efficiency- and background-corrected measured $e^{+}e^{-}$ invariant-mass distribution for opening angles $> 9°$ (*full circles*) compared to a PLUTO simulated di-electron cocktail. The included sources of di-electrons are indicated. Only statistical error bars are shown

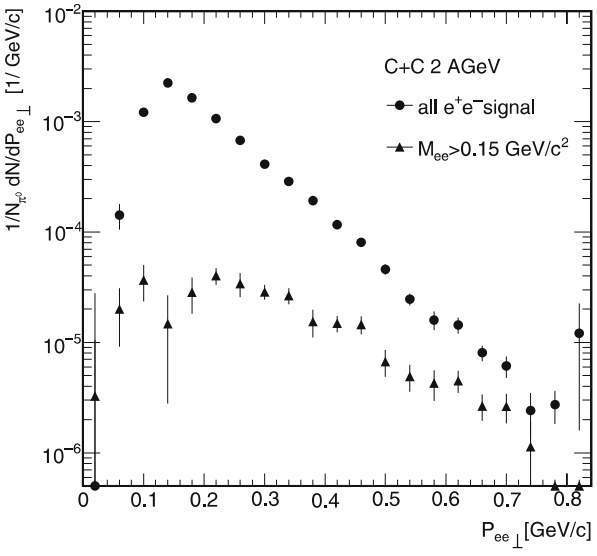

Fig. 4. Transverse momentum distribution of all $e^{+}e^{-}$-signal pairs including efficiency corrections (*circles*) and only for pairs with $M > 0.15\,\mathrm{GeV/c^2}$ (*triangles*). Only statistical error bars are shown

non-trivial radiation from the early phase of the fireball. Multi-step processes with intermediate baryon resonances and off-shell effects play an important role (see [30] for a review). Hence, it was attempted to include vector-meson production in the PLUTO simulation. At this energy, however, the production rates of the light vector mesons ρ and ω are unknown to a large extent. As a first estimate we made use of m_{T} scaling [31] and vacuum spectral functions. The dashed line in Fig. 3 shows the result-

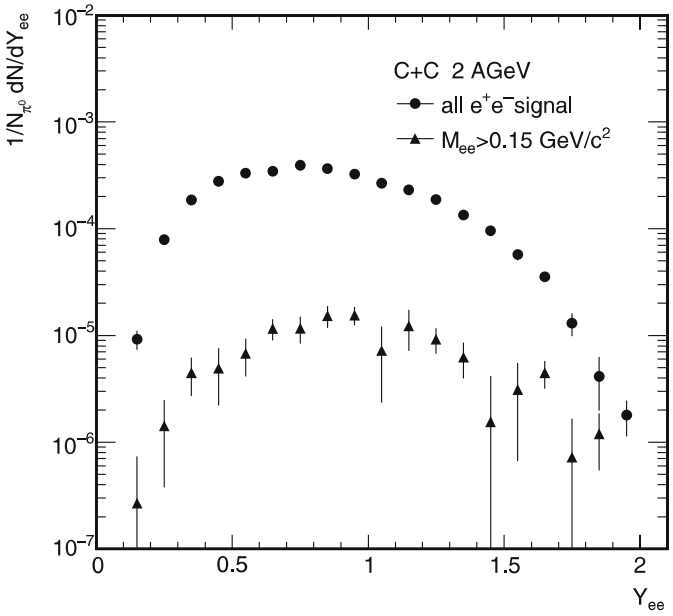

Fig. 5. Rapidity distribution of all e^+e^--signal pairs including efficiency corrections (*circles*) and only for pairs with $M > 0.15\,\mathrm{GeV/c^2}$ (*triangles*). Only statistical error bars are shown

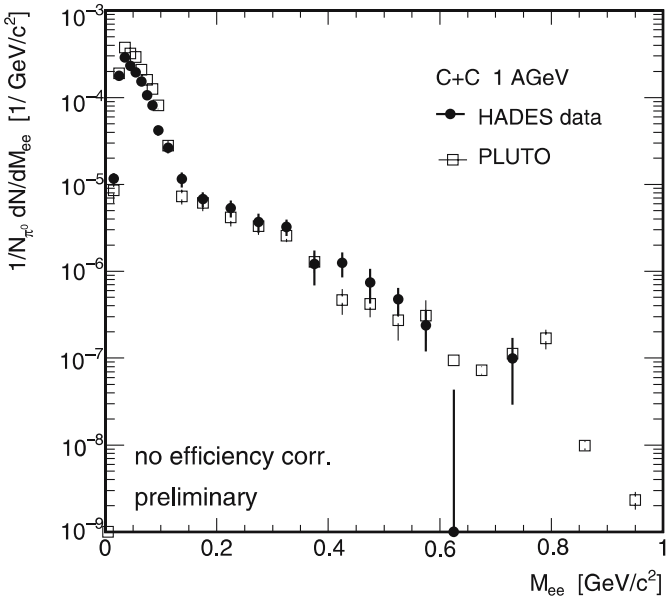

Fig. 6. Reconstructed invariant-mass signal e^+e^--pair distribution from C+C at $E = 1$ AGeV (*full circles*). The spectrum is normalized to the number of measured neutral pions N_{π^0}. The error bars are only statistical. Overlayed is the result of a full GEANT simulation using PLUTO events (*open squares*). No efficiency correction was applied

ing pair distribution including ρ, ω, and Δ resonance decays. The modified ρ shape visible in the decomposition results purely from the thermalisation ansatz which enhances the low-mass tail of the ρ due to the reduced phase space for higher masses close to threshold in 2 AGeV collisions. The pair yield from $\Delta^{0(+)} \to Ne^+e^-$ decays was derived with a calculated branching ratio for this Dalitz decay [12] and under the assumption that the Δ yield scales with the π^0 yield. The simulation now populates the high-mass region above $0.6\,\mathrm{GeV/c^2}$ with di-electrons from vector meson two-body and Dalitz ($\omega \to \pi^0 e^+e^-$) decays, but overestimates the data at the vector-meson mass pole. In the intermediate-mass region, $0.2 < M < 0.6\,\mathrm{GeV/c^2}$, the yields obtained in our cocktail parametrisation are still lower by roughly a factor two as compared to the measured data. This finding clearly indicates the need for a fully microscopic treatment of the collision dynamics.

3.2 C+C at $E = 1$ AGeV

In a second experiment the collaboration has also measured the di-electron production in the C+C system at a projectile energy of $E = 1$ AGeV. The experimental set-up and conditions were similar to the ones described above, with the exception of newly installed outer drift chambers. The recorded data sample corresponds to about 8.4×10^8 inspected collisions. The result of a preliminary analysis is displayed in Fig. 6. In this analysis tracking algorithms for high-resolution momentum reconstruction could be used for the first time, since the outer MDC planes were operational. The particle identification was performed with the probabilistic approach based on Bayes' theorem. At this stage, however, the measured invariant-mass distribution of the net e^+e^- pair signal (i.e. after background subtraction) is not yet efficiency corrected. For a preliminary comparison we have generated an event sample from a cocktail of primary sources in the same way as for the $E = 2$ AGeV case. Due to the lower collision energy, which for free nucleon-nucleon collisions is well below the η - meson production threshold, the abundance of η- and ρ/ω mesons is considerably reduced. The e^+e^--yield from the ρ meson now dominates at intermediate masses due to the chosen thermalisation ansatz. The event sample was propagated through a full GEANT detector simulation and analyzed in the identical way as the data. The comparison to the data reflects that no significant signal is seen in the ρ/ω mass region. At this stage of the analysis further conclusions , in particular concerning the intermediate mass range, cannot be drawn. However, it was carefully checked that the shape of the invariant-mass distribution does not change between the high and low resolution tracking mode. Hence, one can conclude that systematic effects related to the low-resolution mode are small, which is an important fact for the analysis and interpretation of the C+C data at $E = 2$ AGeV.

4 Di-electron production in p+p collisions at $E = 2.2$ GeV

The physics program of the HADES collaboration contains the study of e^+e^--production in elementary reactions as one of the basic ingredients to understand the data measured in heavy ion reactions. One of the aspects is the

verification of di-electron reconstruction efficiencies from reactions in which sources are produced with well known cross sections. For this reason, the collaboration performed a p+p run at an incident energy of E = 2.2 GeV. A beam of typically $2-4\times10^7$ protons per second was directed to a 5 cm thick liquid hydrogen target. The experiment was performed with the outer MDC tracking set-up complete. A high-precision momentum reconstruction based on the Runge-Kutta method was implemented and the invariant-mass resolution could be improved to $\sigma_M/M = 2.4\%$. In a first preliminary analysis we have constructed e^+e^- invariant-mass distributions for the inclusive di-electron production. The net e^+e^-- pair signal normalized to the number of triggered events is shown in Fig. 7. The data points of the C+C system at $E = 2$ AGeV are shown for comparison, after normalisation to the same π^0 yield. The distributions are not corrected for efficiency. It can be noted that both distributions have similar or even identical shapes up to $M \approx 0.35\,\mathrm{GeV/c^2}$. For higher invariant masses, the pair yield measured in the C+C system systematically exceeds the one reconstructed in the pp system, although measured at a lower beam energy. This observation confirms the findings discussed in the previous chapter that the influence of multi-step processes present only in the ion–ion collision scenario are particularly important for the proper description of the e^+e^-- production in the C+C system. However, quantitative conclusions can only be drawn after efficiency corrections have been applied and a comparison to more refined theoretical models has been performed.

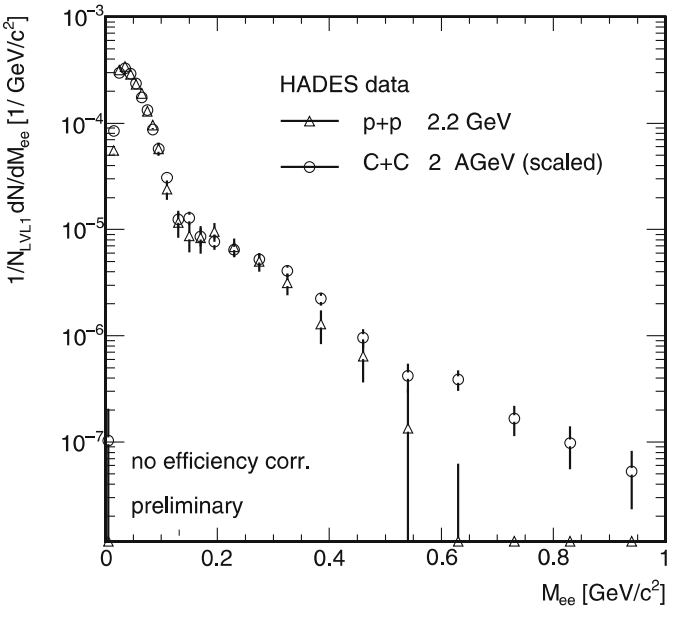

Fig. 7. Comparison of the invariant-mass distribution of unlike-sign signal pairs measured in p+p collisions at 2.2 GeV (*open triangles*) and C+C at 2 AGeV (*open circles*), normalized to the number of the p+p LVL1 events. The C+C data has been normalized to the same π^0 yield. Note that the distributions are not corrected for efficiency

5 Summary and outlook

For the first time the inclusive di-electron production in ^{12}C+^{12}C collisions at $E_{\mathrm{beam}}^{\mathrm{kin}} = 2$ AGeV was measured. A comparison to a simulation using known production and decay rates shows agreement for low masses, but an excess of at least a factor 2 in the intermediate mass range. In the high vector meson mass region m_T scaling clearly overestimates the measured data. The presented preliminary data measured in p+p collisions at a slightly higher beam energy and their comparison to the C+C system underline the importance of multi-step processes for e^+e^--production only accessible in ion collisions. HADES continues its investigations on di-electron production at moderate beam energies. High resolution and high statistics data from a measurement of the collision system Ar+KCl at $E = 1.78$ AGeV is currently being analyzed. A recently completed p+p run at $E = 1.25$ GeV and an upcoming measurement of p+p at $E = 3.5$ GeV will complement the systematic study of this important reference system.

Acknowledgements. The collaboration gratefully acknowledges the support by BMBF 06TM970I, 06GI146I, 06F-140, and 06DR120 (Germany), GSI (TM-FR1,GI/ME3,OF/STR), KBN 5P03B 140 20 (Poland), INFN (Italy), CNRS/IN2P3 (France), GA CR 202/00/1668 and GA AS CR IAA1048304 (Czech Republic), UCY-10.3.11.12 (Cyprus), MCYT FPA2000-2041--C02-02 and XUGA PGID T02PXIC20605PN (Spain), INTAS 03-51-3208 and EU contract RII3-CT-2004-506078.

References

1. G.E. Brown, M. Rho, Phys. Rev. Lett. **66**, 2720 (1991)
2. G.E. Brown, Phys. Rep. **269**, 333 (1996)
3. T. Hatsuda, S.H. Lee, Phys. Rev. C **46**, R34 (1992)
4. B. Friman, H.J. Pirner, Nucl. Phys. A **617**, 496 (1997)
5. CERES Collaboration, G. Agakichiev et al., Eur. Phys. J. C **41**, 475 (2005)
6. M. Masera, Nucl. Phys. A **590**, 93c (1995)
7. NA60 Collaboration, R. Arnaldi et al., Phys. Rev. Lett. **96**, 162 302 (2006)
8. D. Trnka et al., Phys. Rev. Lett. **94**, 192 303 (2005)
9. M. Naruki et al., Phys. Rev. Lett. **96**, 092 301 (2006)
10. DLS Collaboration, R.J. Porter et al., Phys. Rev. Lett. **79**, 1229 (1997)
11. W.K. Wilson et al., Phys. Rev. C **57**, 1865 (1998)
12. C. Ernst et al., Phys. Rev. C **58**, 447 (1998)
13. C. Fuchs, A. Fässler, Prog. Part. Nucl. Phys. **53**, 59 (2004)
14. E.L. Bratkovskaya, C.M. Ko, Phys. Lett. B **445**, 265 (1999)
15. K. Shekhter et al., Phys. Rev. C **68**, 014 904 (2003)
16. M.D. Cozma, C. Fuchs, E. Santini, A. Fässler, nucl-th/0601059
17. R. Schicker et al., Nucl. Instrum. Methods A **380**, 586 (1996)
18. A. Agakichiev et al., Nucl. Instrum. Methods, to be published
19. K. Zeitelhack et al., Nucl. Instrum. Methods A **433**, 201 (1999)

20. M. Böhmer et al., Nucl. Instrum. Methods A **471**, 25 (2001)
21. H. Bokemeyer, et al., Nucl. Instrum. Methods A **477**, 397 (2002)
22. C. Agodi et al., Nucl. Instrum. Methods A **492**, 14 (2002)
23. A. Balanda et al., Nucl. Instrum. Methods A **531**, 445 (2004)
24. J. Lehnert at al. , Nucl. Instrum. Methods A **502**, 261 (2003)
25. A. Toia et al., Nucl. Instrum. Methods A **502**, 270 (2003)
26. S. Bass et al., Prog. Part. Nucl. Phys. **41**, 225 (1998)
27. TAPS Collaboration, R. Averbeck et al., Z. Phys. A **359**, 65 (1997)
28. F. Laue et al., Eur. Phys. J. A **9**, 397 (2000)
29. M.A. Kagarlis, GSI Report 2000-03 (2000), unpublished
30. W. Cassing, E.L. Bratkovskaya, Phys. Rep. **308**, 65 (1999)
31. E.L. Bratkovskaya, W. Cassing, U. Mosel, Phys. Lett. B **424**, 244 (1998)